PAPER

In-Petri-dish traveling and standing acoustic wave-assisted fabrication of anisotropic collagen hydrogels

Yingshan Du, [iD] [a] Jiali Li, [iD] [b] Chongpeng Qiu, [iD] [b] Liang Shen, [b] Teng Li, [iD] [b] Bowen Cai, [iD] [b] Luyu Bo [iD] [b] and Zhenhua Tian [iD] *[b]

Anisotropic biomaterials containing oriented collagen fibers have shown great potential for various biomedical research areas, such as wound dressing, corneal grafting, and the study of cancer cell invasion in biomimetic microenvironments. To fabricate such anisotropic biomaterials, previous studies have used electric, microfluidic, magnetic, and mechanical methods to align collagen fibers during the fabrication process. In this study, we put forward traveling and standing acoustic wave-based approaches that enable the rapid in-Petri-dish fabrication of anisotropic biomaterials containing acoustically arranged collagen fibers. To develop these approaches, we investigated the effects of traveling and standing acoustic waves on collagen self-assembly and the micro/nanoscale architectures of the fabricated collagen-based biomaterials. Our results reveal that traveling acoustic wave-induced fluid streaming can transport collagen molecules, thereby influencing the collagen self-assembly process, while standing acoustic waves can accumulate self-assembled collagen fibers, increasing their concentrations in acoustic potential valleys periodically distributed. Using our acoustics-assisted approach, we successfully manufactured anisotropic collagen hydrogels containing aligned collagen fibers, which provide anisotropic microenvironments for cell growth and development. Notably, we demonstrated the functionality of these fabricated anisotropic collagen hydrogels in facilitating cell elongation along the acoustically aligned collagen fibers. Compared to previous methods, our acoustics-based approaches are easy to operate without requiring customized chambers for loading collagen and are capable of rapidly fabricating anisotropic collagen hydrogels directly in commercial Petri dishes, thus allowing our approaches to be readily integrated into existing laboratory workflows and combined with other test protocols. In the long run, we expect this work to inspire the development of useful tools that will benefit biomedical researchers working in tissue engineering, regenerative medicine, biomaterials, and bioprinting.

1. Introduction

Biomaterials containing collagen fibers have garnered increasing attention in various research fields, such as tissue engineering,[1,2] bioprinting,[3,4] tumor research,[5,6] and wound healing.[2,7] The internal collagen fibers play a pivotal role in affecting the mechanical properties of biomaterials,[8] creating biomimetic physiological environments,[9] and modulating biological processes such as tumor progression,[10] and cell migration,[11,12] signaling,[13–15] and differentiation.[16,17] In native tissues, such as muscle tendons,[18,19] cornea,[20] bone,[21,22] and skin,[23] collagen fibers exhibit various arrangements, contributing to the distinct material properties

and functions of these tissues. In muscle tendons, collagen fibers are organized into clustered bundles aligned along the direction of muscle contraction, contributing to the mechanical properties and tissue function.[24] Native corneas have multiple layers of collagen fibers oriented in different directions, contributing to their unique mechanical and optical properties.[25] In wound healing, the regenerated scar tissue is found to have collagen fibers in parallel orientation.[26,27] The tumor extracellular matrix features aligned collagen architectures that have been shown to facilitate cancer metastasis.[28] Collagen fiber orientation in bone affects the bone's mechanical properties and mineralization process and can vary depending on the type of bone tissue. For example, collagen fibers exhibit a plywood-like arrangement in lamellar bone, increasing the bone's strength in multiple directions, and collagen fibers in long bones are predominantly oriented along the longitudinal axis to enhance tensile strength.[29]

[a] Department of Biomedical Engineering and Mechanics, Virginia Polytechnic Institute and State University, Blacksburg, VA, 24060, USA

[b] Department of Mechanical Engineering, Virginia Polytechnic Institute and State University, Blacksburg, VA, 24060, USA. E-mail: tianz@vt.edu

Because of the aforementioned pivotal roles of collagen fiber arrangements, there is increasing interest in developing technologies to manufacture biomaterials containing organized collagen fibers for tissue engineering, as well as for fundamental research on the effects of collagen fiber arrangements on biological processes.[30] Multiple methods have been established to arrange collagen fibers and assist in the fabrication of collagen-based biomaterials, such as those based on electrospinning,[31,32] microfluidics,[33–39] mechanical loading,[40–43] electric fields,[44–50] and magnetic fields.[51–54] Among these, the magnetic method requires incorporating magnetic beads into collagen solutions; however, these beads are difficult to remove from collagen hydrogels.[55,56] The electric approach requires a customized thin chamber with an anode and a cathode to apply a strong electric field for collagen fiber alignment.[57] Mechanical loading is typically used as a post-treatment step to cyclically stretch fabricated collagen hydrogels.[58] Microfluidic techniques require customized microchannels for effective collagen fiber alignment.[59] Despite the success of these methods in arranging collagen fibers, none can conveniently arrange collagen fibers within Petri dishes, which are common laboratory supplies, for the quick fabrication of customized biomaterials containing organized collagen fibers. We believe that a technology filling this gap could be more easily integrated into existing laboratory workflows and combined with other test protocols, benefiting researchers working in tissue engineering and bioprinting applications, as well as fundamental studies on the effects of collagen fiber arrangements on biological processes.

Acoustics-based techniques for manipulating micro/nano-sized objects[60–65] have shown great potential for biomedical, biological, and chemical research due to their biocompatible, non-invasive, contactless, and label-free features. For example, acoustic waves have been successfully used to manipulate objects of different sizes, such as exosomes,[66] cells,[67,68] bacteria,[69] and zebrafish larvae,[70,71] and have been applied in applications such as cell sorting[72,73] and cell separation,[74,75] and drug delivery.[76,77] Additionally, some studies demonstrated the ability of using acoustic waves for aligning collagen fibers.[78–81] Zhang *et al.* successfully aligned collagen fibers in a microfluidic chamber using an electric field, which were induced by high-frequency standing surface acoustic waves generated on a lithium niobate piezoelectric wafer.[80] However, this approach primarily relied on the dielectrophoretic forces, and the effects of acoustic radiation force and streaming were not investigated. Norris *et al.* used an ultrasound transducer in a bulky water bath tank to influence collagen fiber arrangement in a multi-well plate placed on the top surface of the bath.[78,79,81] This setup was difficult to integrate with inverted microscopes for real-time observation of the collage fiber arrangement process. They demonstrated that collagen fibers could be arranged in a radial distribution surrounding a collagen-absent region[79] and suggested that the underlying mechanism for collagen arrangement might involve acoustic streaming or cavitation. However, key experiments, such as acoustic streaming field measurements and real-time visualization of the collagen arrangement process, were not conducted

to clearly elucidate the ultrasound-induced collagen alignment mechanism. Additionally, the effects of standing bulk acoustic waves on collagen self-assembly and fiber arrangement were not covered in those studies.[78–81]

In this study, we established traveling and standing acoustic wave-based approaches that enable the rapid fabrication of anisotropic biomaterials containing acoustically arranged collagen fibers directly in Petri dishes. Moreover, we unveiled the effects of traveling wave-induced streaming and standing waves on collagen self-assembly in Petri dishes, as well as the distribution and orientation of collagen fibers in fabricated collagen hydrogels. Through experiments, we found that acoustic streaming generated by traveling acoustic waves can transport collagen molecules, thereby affecting the self-assembly of collagen in Petri dishes. This mechanism enables a traveling acoustic wave-assisted approach for fabricating anisotropic collagen hydrogels with oriented collagen fibers in Petri dishes. On the other hand, our experimental results reveal that standing acoustic waves can increase the concentrations of self-assembled collagen fibers in periodically distributed acoustic potential valleys. This mechanism enables a standing acoustic wave-assisted approach for in-Petri-dish fabrication of collagen hydrogels with periodically and parallelly arranged macro-bundles densely packed with collagen fibers. Compared to previous methods for fabricating biomaterials with organized collagen fibers,[6,82] our acoustics-based approaches are easy to operate and compatible with microscopes for real-time observation and allow for rapid fabrication directly in commercial Petri dishes, making them more readily integrated into existing laboratory workflows and easily combined with other test protocols requiring organized collagen fibers.
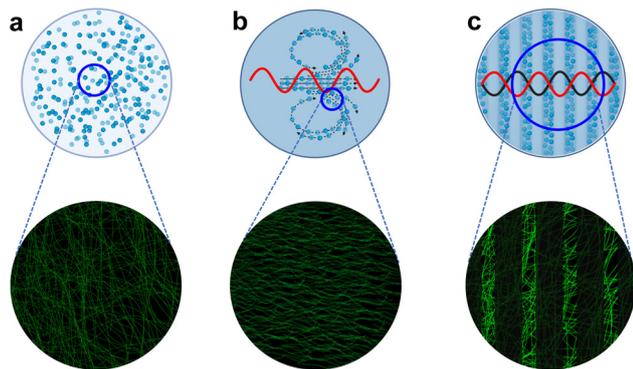
2. Results and discussion

2.1 Mechanisms of traveling and standing acoustic wave-assisted fabrication of anisotropic collagen hydrogels

In the fabrication of collagen hydrogels, the self-assembly of collagen molecules typically leads to randomly distributed collagen fibers, as illustrated in Fig. 1(a). This self-assembly process lacks an active force field exerting on collagen molecules to control their distributions during assembly. Acoustic waves propagating through fluids are known to apply acoustic radiation forces on micro/nano-sized objects in fluids, as well as generate acoustic streaming (*i.e.*, fluid flow), which can apply drag forces on these in-fluid objects.[83] In particular, this study finds that acoustic wave-induced potential valleys and drag forces have the potential to actively control the collagen self-assembly process, enabling the rapid and easy-to-operate fabrication of anisotropic collagen hydrogels in commercial Petri dishes.

Since traveling and standing acoustic waves lead to different acoustofluidic phenomena, such as directional streaming flows and an array of potential wells arranged periodically, we investigated the effects of both traveling and standing acoustic waves on collagen self-assembly, specifically their effects on the orientations of assembled collagen fibers and the micro/

Fig. 1 Schematics illustrate the mechanisms of traveling and standing acoustic wave-assisted fabrication of anisotropic collagen hydrogels. (a) Without acoustic waves, the self-assembly of collagen molecules results in randomly distributed collagen fibers. (b) With traveling acoustic waves, acoustic streaming is generated, transporting collagen molecules and resulting in aligned collagen fibers after self-assembly. (c) With standing acoustic waves, the self-assembled collagen fibers tend to group together in the acoustic potential valleys, forming a periodic pattern with regions of low and high collagen concentrations.

nanoscale architectures of fabricated collagen hydrogels. As illustrated in Fig. 1(b), in-liquid traveling waves, typically generated by a single transducer, can induce a directional acoustic streaming flow parallel to the acoustic wave propagation direction. When the directional streaming flow encounters the Petri dish wall, the flow direction alters, creating a pair of reflux flows, which further lead to a pair of counter-chirality streaming vortices. During collagen self-assembly, the streaming flow can transport collagen molecules along its direction, thereby influencing the collagen self-assembly process, the orientations of collagen fibers, and the micro/nanoscale architectures of the fabricated collagen hydrogels. This study, in particular, finds that the self-assembled collagen fibers tend to align along the streaming flow direction, demonstrating the potential of using traveling acoustic wave-induced acoustofluidic streaming to align collagen fibers and fabricate anisotropic collagen hydrogels.

In contrast to traveling acoustic waves, in-liquid standing acoustic waves, typically generated by a pair of parallelly arranged transducers, have parallelly arranged, periodic acoustic potential peaks and valleys to exert periodic acoustic force fields on in-liquid particles. With these features, standing acoustic waves are capable of arranging small particles in periodic patterns. Therefore, applying standing acoustic waves during the collagen self-assembly process affects the final arrangement of collagen fibers and the micro/nanoscale architecture of the fabricated hydrogels. Particularly, this study finds that the self-assembled collagen fibers tend to group together in the acoustic potential valleys, facilitating the fabrication of collagen hydrogels containing low and high collagen concentrations in periodic patterns, as illustrated in Fig. 1(c).

To elucidate the mechanisms by which traveling and standing acoustic waves control the collagen self-assembly process, we designed test devices compatible with commercial Petri dishes, characterized the acoustic and fluid streaming fields

generated in Petri dishes using laser Doppler vibrometry and particle image velocimetry, respectively, and investigated the effects of traveling and standing waves on collagen self-assembly. The arrangement of collagen fibers in the manufactured collagen hydrogels was characterized by confocal imaging. Key results are presented in the following subsections of Results and Discussion, and their related experimental procedures are detailed in the Experimental section.

2.2 Design and characterization of devices for acoustics-assisted in-Petri-dish collagen hydrogel manufacturing

To investigate the effects of traveling and standing acoustic waves on collagen self-assembly and to achieve acoustics-assisted in-Petri-dish collagen hydrogel fabrication, we designed test devices (illustrated in Fig. 2(a)) composed of plate-type piezoelectric transducers (PZTs) and commercial Petri dishes, which serve as the chambers for acoustic field generation and collagen molecule manipulation. When a single transducer is dipped into the solution loaded in a Petri dish (Fig. 2(a), left), traveling acoustic waves, as well as their resulting acoustic streaming, are generated. When a pair of parallel transducers are dipped into the solution in a Petri dish (Fig. 2(a), right), standing acoustic waves with parallelly
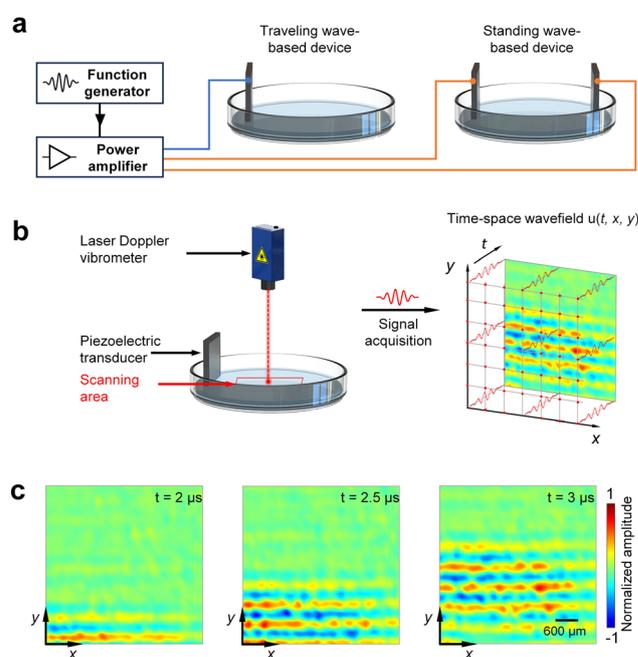
Fig. 2 Acoustic device design and characterization. (a) Experimental setup schematics for using traveling acoustic waves generated by a piezoelectric transducer and standing acoustic waves generated by a pair of transducers to influence the self-assembly of collagen molecules loaded in Petri dishes. The piezoelectric transducers are excited by harmonic signals generated by a function generator and amplified by a power amplifier. (b) Schematic of the setup for characterizing pressure acoustic waves generated by a piezoelectric transducer propagating in a liquid layer in a Petri dish. Through point-by-point scanning, the laser Doppler vibrometer can acquire a time-space wavefield u (t, x, y). (c) Acquired wavefield at different time points showing the propagation of straight wavefront pressure acoustic waves in a Petri dish.

arranged potential valleys are generated. Notably, our approach is compatible with commercial Petri dishes, avoiding the need for customized chambers compared to electric and microfluidic methods.[34,84,85] Additionally, the acoustics-assisted collagen hydrogel fabrication devices can be placed on the translation stages of either inverted or upright microscopes, allowing for easy real-time observation of acoustic effects on the collagen hydrogel gelation process.

Before applying our devices to control collagen self-assembly, we characterized the acoustic transducers' operating frequencies using a network analyzer, the generated acoustic fields using a laser Doppler vibrometer, and the generated streaming fields using particle image velocimetry. The network analyzer revealed the first- and second-order resonance frequencies of the transducer at 3.09 and 9.60 MHz. To measure the high-resolution acoustic fields generated in a liquid layer preloaded into a Petri dish, we used a laser vibrometry setup illustrated in Fig. 2(b). A function generator was used to excite the transducer to generate acoustic waves in a thin liquid layer in a Petri dish. A laser Doppler vibrometer directed a laser beam perpendicularly through the liquid layer, which then reflected back from a reflective tape placed under the Petri dish. The acoustic waves propagating in the liquid layer affected the laser beam transmission, enabling the characterization of acoustic waves overlapping with the laser path, similar to previous studies on measuring pressure acoustic waves in water.[86] By adjusting the laser head position with a linear motion stage and performing measurements at multiple points on a two-dimensional grid, a multi-dimensional time-space wavefield u (t, x, y) was acquired, revealing the propagation of the generated acoustic waves. Fig. 2(c) shows the acquired acoustic pressure fields at different times when the transducer was excited with a tone burst signal at a frequency of 3.09 MHz (i.e., the transducer's first-order resonance frequency). These results confirm the successful generation of directional traveling pressure acoustic waves with parallel wavefronts in the liquid layer loaded in a Petri dish. Additionally, a needle-type hydrophone (HNR-0500, ONDA Co.) was used to characterize the acoustic pressure in the Petri dish. We found that the acoustic pressure increased from approximately 10 to 15 kPa when the excitation voltage of the piezoelectric transducer was raised from 7 to 10 V.

To characterize the acoustic streaming field, particle image velocimetry was performed. The motions of 5-μm green, fluorescent tracing particles, induced by acoustic streaming, were recorded by a camera attached to an inverted microscope. The acquired time-sequential fluorescent microscopy images were then processed using particle image velocimetry analysis[87,88] to obtain the streaming velocity field. Fig. 3(a) shows an image obtained by stacking a series of images acquired at different times when the transducer was excited at 3.09 MHz with a voltage of 8 V. As the traveling wave-induced acoustic streaming field in a round Petri dish is symmetric with respect to the wave propagation direction, Fig. 3(a) only shows the result acquired from one side of the flow field. Fig. 3(b) presents the acquired streaming velocity field, with the arrows indicating streaming velocity directions and the image intensities representing streaming velocity magnitudes. These results reveal a predominant unidirectional flow near the center of the Petri dish, a vortex flow near the dish's side induced by reflux, and a transition region between the vortex and the central unidirectional flow. Movie S1 shows particle motions in three regions of the streaming field, including the vortex streaming region, transition region, and central directional flow region. The generated streaming field in the Petri dish is influenced by the transducer's position, resonance mode shape, and excitation signal power. Therefore, the streaming field can be modified through several approaches, including adjusting the transducer's position; changing the input frequency to excite different resonance modes (such as in-plane and out-of-plane modes), each with distinct mode shapes; and tuning the input power of the transducer. As shown in Fig. 3(c), the average streaming velocity in the central flow region gradually increases as the excitation voltage of the piezoelectric transducer rises from 7 to 10 V. In contrast, the streaming velocity decreases with increasing collagen concentration (from 0.5 to 2.5 mg mL^{-1}) due
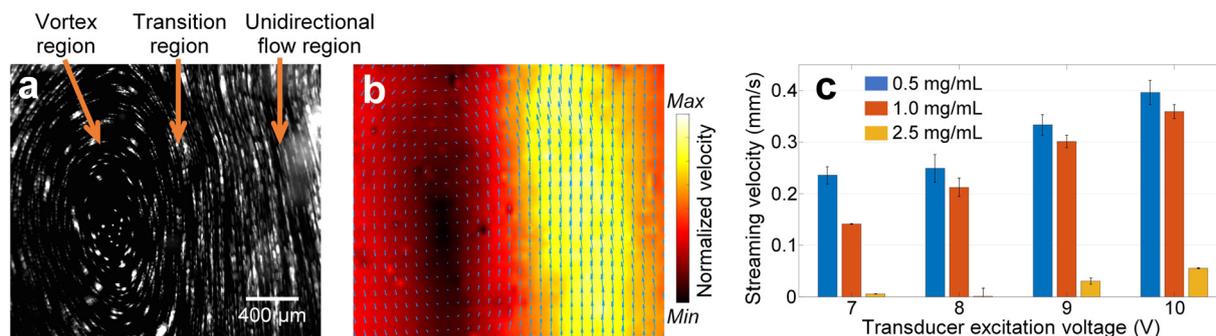

Fig. 3 Characterization of traveling acoustic wave–induced fluid streaming in a Petri dish. (a) A stacked microscopic image revealing the motions of fluorescent tracing particles induced by acoustic streaming. (b) Streaming velocity field obtained through particle image velocimetry. The velocity magnitude distribution is indicated by the intensity field, and the streaming flow directions are indicated by the arrows. These results reveal a unidirectional flow region near the center of the dish, a vortex streaming region off-center, as well as a transition region in between. (c) Streaming velocities in the unidirectional flow region for cases with different transducer excitation voltages and collagen concentrations. The streaming velocity increases with increasing excitation voltage (from 7 to 10 V), but decreases with increasing collagen concentration (from 0.5 to 2.5 mg mL^{-1}).

to the higher viscosity of the collagen solution. The effects of transducer position and resonance mode shape on the streaming fields are beyond the scope of this work and will be investigated in future studies.
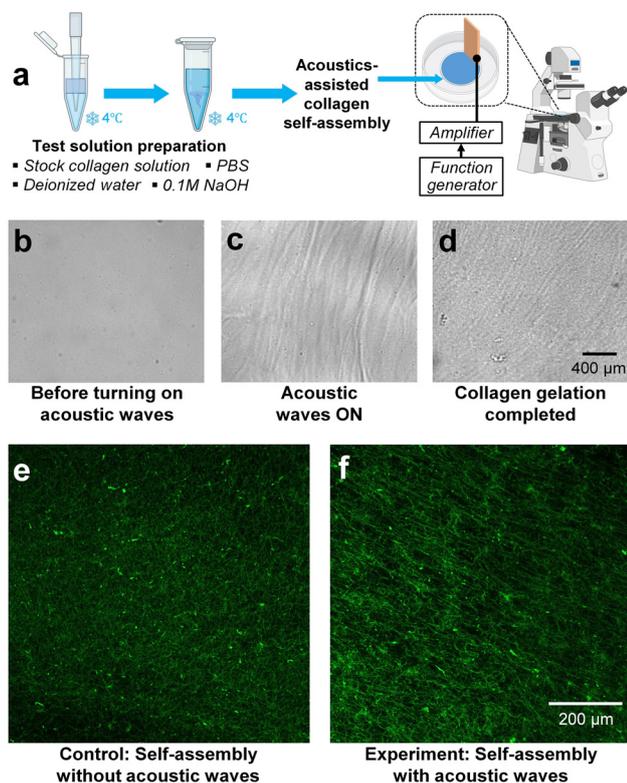
2.3 Traveling acoustic wave effects on collagen self-assembly

To investigate the effects of traveling acoustic waves on collagen self-assembly, we used a device with a piezoelectric transducer dipped into the collagen solution loaded in a Petri dish (see Fig. 2(a)). After gelation, the fabricated collagen hydrogels were characterized using confocal imaging to analyze the collagen fiber orientations and the hydrogels' internal micro/nanoscale architectures. The diagram in Fig. 4(a) illustrates the key test procedures. A stock solution of type I collagen (concentration 5 mg mL^{-1}) was diluted with deionized water, neutralized with 0.1 N NaOH, and mixed with phosphate-buffered saline to obtain test solutions with varying concentrations, such as 0.5, 1.0, and 2.5 mg mL^{-1}. The preparation step was performed on ice to maintain a low temperature (~ 4 °C). The prepared test solution was quickly added into a Petri dish, which was then placed on the microscope stage for real-time monitoring of the

Fig. 4 Results show the effects of traveling acoustic waves on collagen self-assembly and gelation. (a) Schematics illustrate key steps for preparing collagen test solutions and the setup for traveling acoustic wave-assisted collagen self-assembly. (b)–(d) Brightfield microscopic images acquired at different time points: before turning on acoustic waves, after turning on acoustic waves, and after collagen gelation. (e) and (f) Confocal fluorescent microscopic images of the fabricated collagen hydrogels showing randomly distributed collagen fibers in the control group (without acoustic waves) and collagen fibers with clear directionality in the experimental group (with acoustic waves).

collagen gelation process. A piezoelectric transducer was dipped into the collagen solution and activated to generate traveling acoustic waves and acoustic streaming, thereby influencing the collagen self-assembly process. After 5–10 min, the liquid collagen solution transformed into a collagen hydrogel containing self-assembled collagen fibers. In this process, the piezoelectric transducer excited at 10 V generated a small amount of heat, which slightly increased the temperature of the collagen solution to approximately 26.5 °C, as measured by a thermal camera (TIM-400, Micro-Epsilon). This temperature rise accelerated the collagen self-assembly process and the transformation from a solution to a hydrogel without causing collagen denaturation.[89,90] This observation is consistent with previous studies, which found that type I collagen undergoes entropy-driven self-assembly when the temperature of a neutralized collagen solution rises above 25 °C.[30,33,41]

Fig. 4(b)–(d) show images acquired before, during, and after the collagen self-assembly process. Before activating the acoustic waves, collagen molecules were randomly distributed in the liquid phase (see Fig. 4(b)). After the acoustic waves were activated, acoustic streaming propelled the collagen molecules to flow along the streaming direction (see Fig. 4(c)), thereby affecting their self-assembly into collagen fibers. Upon completion of the collagen self-assembly process, the liquid phase transformed into a hydrogel layer, with oriented collagen fibers aligned by acoustic streaming (see Fig. 4(d)). To visualize the traveling wave-assisted collagen gelation process, Movie S2 was recorded during an experiment. It shows that the traveling wave-induced streaming transports collagen macromolecules along the streaming flow. It also shows gelled collagen in the imaging domain's left part (closer to the streaming vortex) where the streaming velocity is relatively lower.

To better reveal the collagen fiber orientations, the fibers in fabricated hydrogels were fluorescently labeled and then analyzed through confocal imaging. Fig. 4(e) and (f) (see Fig. S1a and b for high-resolution images) compare the confocal imaging results of control (acoustics off) and experimental (acoustics on) groups, unveiling the effects of traveling acoustic waves on collagen self-assembly. In the control group, collagen fibers are randomly distributed, whereas, in the experimental group with traveling acoustic waves, the collagen fibers are predominantly aligned by acoustic streaming. Moreover, the collagen fibers in the acoustics on group are mostly stretched compared to the control group, where the fibers exhibit curved morphologies. We also demonstrated the feasibility of our acoustic approach for different collagen concentrations. The results in Fig. 5(a)–(c) (see Fig. S2b–d for high-resolution images) for collagen concentrations of 0.5, 1, and 2.5 mg mL^{-1}, respectively, all show collagen fibers aligned by acoustic streaming, induced by traveling acoustic waves at 3.09 MHz (*i.e.*, the transducer's first-order resonance frequency). In addition, when using traveling acoustic waves at 9.60 MHz (*i.e.*, the transducer's second-order resonance frequency), acoustic streaming was also generated, affecting the collagen gelation process and resulting in a hydrogel containing aligned collagen fibers, as shown in Fig. 5(d) (see Fig. S2e for a high-resolution image).
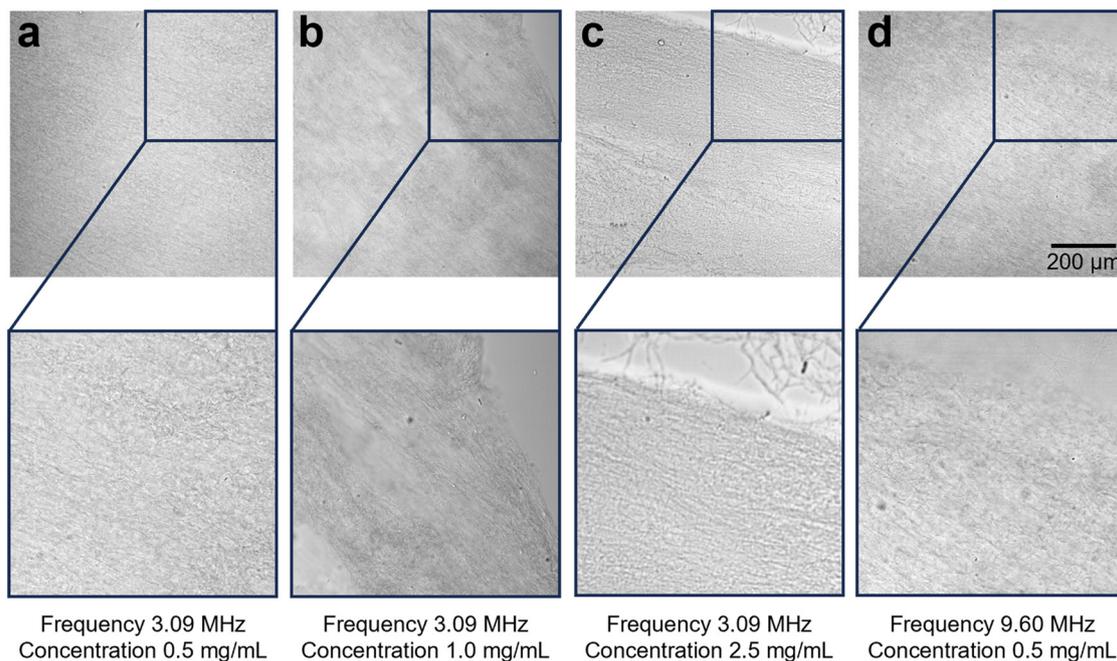
Fig. 5 Microscopic images showing acoustically oriented collagen fibers under different traveling wave frequencies and collagen concentrations: (a) 3.09 MHz waves, 0.5 mg mL^{-1} collagen concentration, (b) 3.09 MHz waves, 1.0 mg mL^{-1} collagen concentration, (c) 3.09 MHz waves, 2.5 mg mL^{-1} collagen concentration, and (d) 9.60 MHz waves, 0.5 mg mL^{-1} collagen concentration.

2.4 Collagen fiber orientations in different regions of a traveling acoustic wave-induced streaming field in a Petri dish

The acoustic streaming field generated in a Petri dish has different streaming directions and velocities, as revealed by the particle image velocimetry results (Fig. 3), exhibiting a unidirectional flow region along the Petri dish's center, a vortex streaming region near the dish's slide, and a transition region between the unidirectional flow and vortex regions. To understand the effects of different acoustic streaming patterns on collagen fiber arrangements, the collagen fiber orientations in these three flow regions were analyzed. Fig. 6(a) shows a stitched brightfield microscopic image acquired after collagen gelation, covering the unidirectional flow region (right), flow transition region (middle), and vortex region (left). From the acquired microscopic image, we analyzed the orientations of collagen fibers in three boxed areas (areas 1 to 3 in Fig. 6(a)),
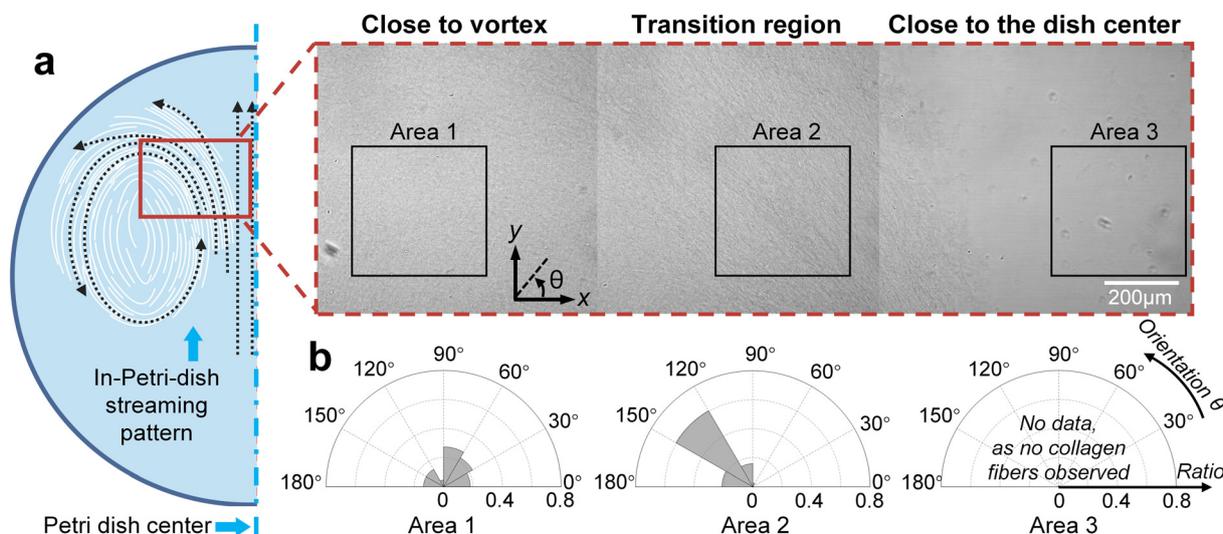

Fig. 6 Characterization of collagen fiber orientations in different regions of the traveling acoustic wave-induced streaming field in a Petri dish. (a) A stitched microscopic image of a fabricated collagen hydrogel showing the collagen fiber orientations in the area near the streaming vortex (left), the transition region (middle), and the area close to the Petri dish's center (right). (b) Polar plots showing collagen fiber directionality analysis results for Areas 1, 2, and 3, indicated by black boxes in (a). No data is shown in the polar plot for Area 3, as collagen fibers are barely observed in that region.

which are within the three regions with different streaming patterns. The results reveal distinct collagen fiber orientations in different regions of the traveling acoustic wave-induced streaming field in a Petri dish. In area 1 located in the vortex streaming region, collagen fibers are oriented in multiple directions without showing clear directionality (see Fig. 6(b), left). In Area 2, within the transition region, the analysis result (Fig. 6(b), middle) shows strong directionality, with the majority of collagen fibers oriented between 120 to 150 deg, correlated to the acoustic streaming flow direction in the flow transition region. In area 3, within the unidirectional flow region, almost no collagen fibers are observed. The absence is attributed to the higher flow velocities in the unidirectional flow region compared to other regions, resulting in the transportation of collagen molecules continuously away from this area.
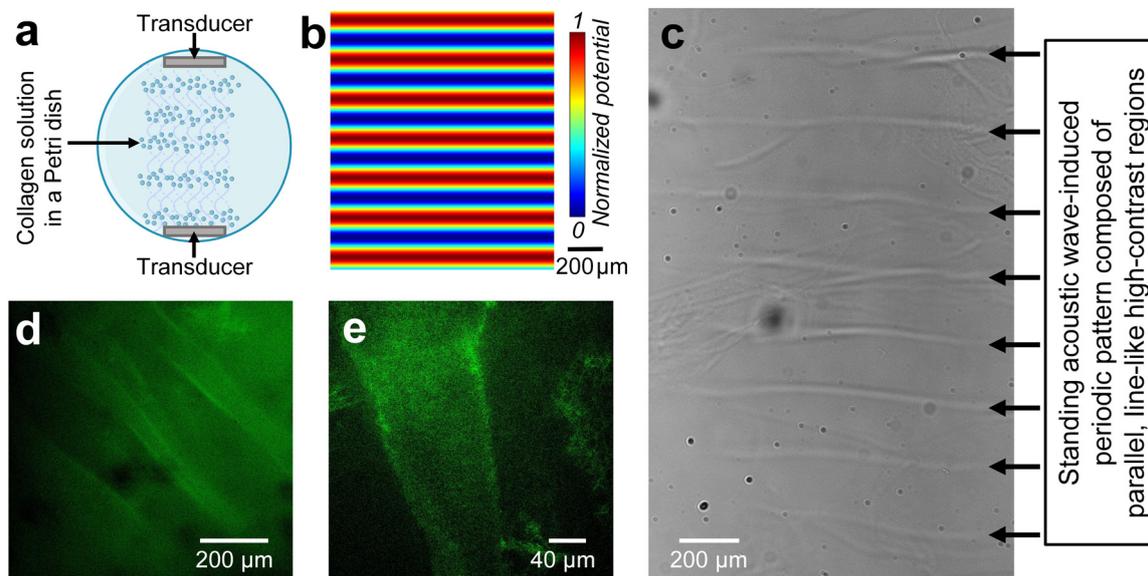
2.5 Standing acoustic wave effects on collagen self-assembly

In addition to traveling acoustic waves, we also experimentally investigated the impact of standing bulk acoustic waves on collagen self-assembly and compared the effects of standing and traveling acoustic waves. Fig. 7(a) illustrates a schematic of the test setup (top view), with a pair of piezoelectric plate-type transducers facing each other in a Petri dish. A collagen solution was added to the Petri dish, and the two piezoelectric transducers were turned on simultaneously to generate standing bulk acoustic waves in the solution. After the completion of collagen gelation in 5–10 min, a collagen hydrogel containing acoustically arranged collagen fibers was obtained. It was then imaged through brightfield and fluorescent microscopy.

In the acquired brightfield microscopic image (Fig. 7(c)), the fabricated collagen hydrogel exhibits a parallel line-like pattern, indicated by multiple line-like high-contrast regions. We also simulated the generated acoustic potential field using an analytical method presented in our previous work.[91] The simulated wavefield of standing acoustic waves at 3.09 MHz showed parallel acoustic potential valleys (Fig. 7(b), blue regions). The spacing between potential valleys in the simulated acoustic field is almost identical to the spacing between the line-like high-contrast regions observed in the brightfield microscopic image. To reveal the collagen fiber distribution, the fabricated collagen hydrogel was stained for fluorescent imaging. The acquired fluorescent images in Fig. 7(d) and (e) show collagen bundles consisting of densely packed collagen fibers, and these bundles are aligned parallel to the potential valleys of the generated standing acoustic waves. However, within each bundle, the small collagen fibers are not well oriented along the potential valley, as shown in Fig. 7(e), implying that the forces applied by 3.09 MHz standing acoustic waves on collagen fibers are not sufficient to control their orientation. As presented above, our experimental results reveal that standing acoustic waves have the potential to increase collagen fiber concentrations in acoustic potential valleys and create parallelly arranged macroscale bundles that are densely packed with nanoscale collagen fibers.
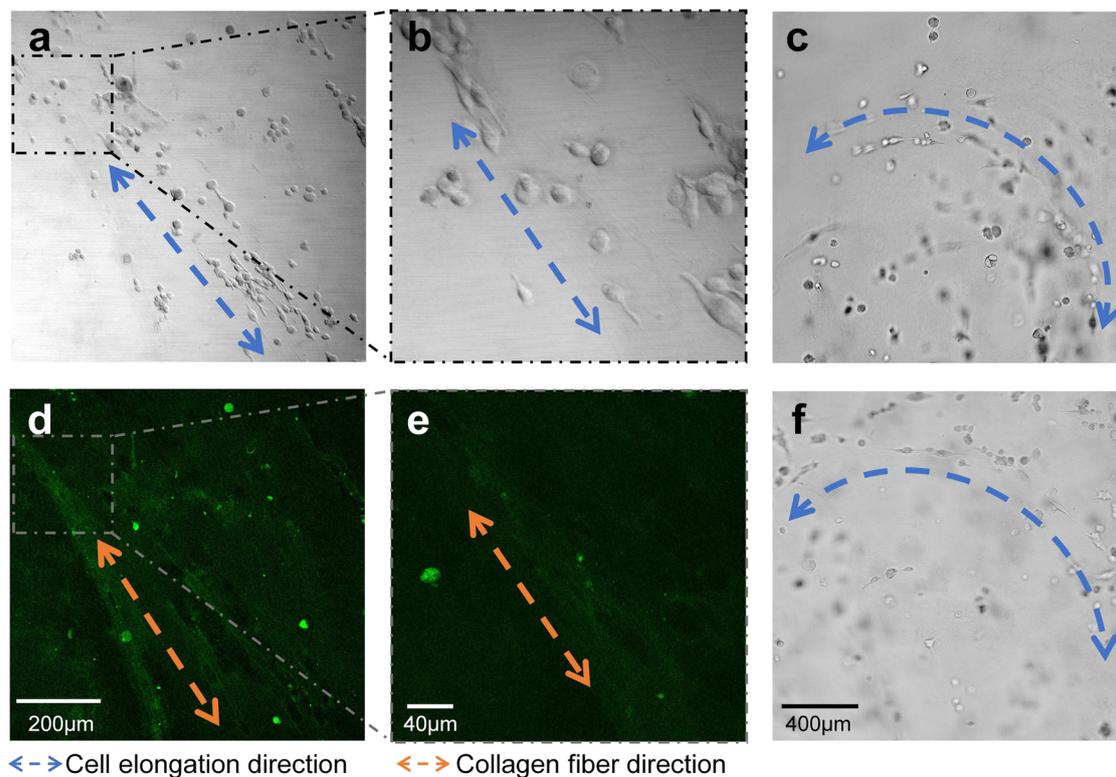
2.6 Cell elongation in hydrogels with aligned collagen fibers

To demonstrate the functionality of collagen hydrogels fabricated by our acoustics-assisted self-assembly approach, human

Fig. 7 Results showing the effects of standing acoustic waves on collagen self-assembly and gelation. (a) Schematic illustrating the test setup with two piezoelectric transducers facing each other to generate standing acoustic waves in a Petri dish loaded with a collagen solution. (b) Analytical simulation result of the generated acoustic potential field at 3.09 MHz, showing parallel, periodic acoustic potential valleys (blue regions). (c) Brightfield microscopic image of a fabricated collagen hydrogel showing parallel, line-like high-contrast regions induced by standing acoustic waves. (d) A confocal image showing multiple bundles formed by acoustically concentrated collagen fibers. (e) A magnified confocal image showing the details of a single bundle containing numerous randomly arranged collagen fibers. These results indicate that standing acoustic waves at 3.09 MHz can increase collagen fiber concentrations at acoustic potential valleys and create collagen fiber bundles.

< - > Cell elongation direction   < - > Collagen fiber direction

Fig. 8 Cell elongation in collagen hydrogels fabricated by acoustics-assisted self-assembly process. Collagen hydrogels contain acoustic streaming aligned collagen fibers. The directions of cell elongation are consistent with the orientation of aligned collagen fibers. (a) and (d) Brightfield and fluorescence microscopy images showing cell elongation and collagen fiber orientation, respectively. (b) and (e) Zoom-in views of (a) and (d), respectively. (c) and (f) Brightfield images showing cell arrangement and elongation in regions with collagen fibers arranged along curved paths in the streaming transition region.

glioblastoma U251 cells were seeded in collagen hydrogels and cultured. We then analyzed the distribution and elongation of cells within these hydrogels, which contained acoustically aligned collagen fibers. Initially, cells were mixed into the collagen solution before activating the traveling acoustic waves for assisted collagen self-assembly. Upon completion of this process, we obtained collagen hydrogels containing both cells and acoustically arranged collagen fibers, which function as scaffolds with oriented nanoscale collagen fibers influencing cell growth. Cells were then cultured within the collagen hydrogel for three days, followed by examining cell growth and morphological changes. The acquired brightfield microscopy images (Fig. 8(a) and (b)) show cell distributions and elongated morphologies. The acquired fluorescence images (Fig. 8(d) and (e)) reveal acoustically aligned collagen fibers. The comparison of cell elongation and collagen fiber orientation indicates that cells predominantly elongate along the aligned collagen fibers, confirming that acoustic wave-induced collagen fiber alignment influences cell growth orientation and morphology. This also indicates that the acoustically aligned collagen acts as guides or scaffolds, providing adhesion sites for embedded cells and guiding the cell growth and elongation. We also demonstrate the potential for guiding cell growth along curved paths by acoustically arranging collagen fibers along curved paths. As shown in Fig. 8(c) and (f), cells in the streaming flow transition region, where collagen fibers are arranged along a curved

trajectory, elongate along that trajectory. The above demonstration proves that collagen hydrogels assembled under acoustic waves can serve as functional biomaterials to regulate cell arrangement and growth direction.

Compared to the traveling wave-based method that induces collagen fiber alignment, the standing wave-based approach achieves different collagen fiber arrangements. Hence, the effects of standing wave-induced collagen fiber arrangements on cell behavior should differ from those of traveling wave-aligned collagen fibers. We hypothesize that cells located in regions with densely packed collagen fibers (within the acoustic potential valleys) experience limited migration due to increased matrix resistance, and the morphologies of these cells tend to be more rounded and compact. In contrast, cells located in regions with lower collagen fiber concentrations (outside the acoustic potential valleys) are more likely to migrate due to lower matrix resistance and tend to spread along local collagen fibers, exhibiting spindle-like morphologies. In future work, we will conduct additional experiments to test these hypotheses and further investigate how collagen architectures induced by standing acoustic waves influence cell behavior.

3. Conclusion

In this study, we investigated the effects of traveling and standing bulk acoustic waves on the self-assembly of collagen

molecules into collagen fibers, for achieving in-Petri-dish fabrication of anisotropic collagen hydrogels. Through experimental studies, on one hand, we found that acoustic streaming generated by traveling acoustic waves can transport collagen molecules in a solution, thereby influencing the collagen self-assembly process, achieving aligned self-assembled collagen fibers along the streaming flow direction, and affecting the micro- and nanoscale architecture of the fabricated collagen hydrogels. Meanwhile, the temperature of the collagen solution slightly increases to approximately 26.5 °C, which accelerates the collagen self-assembly process without causing collagen denaturation.[89,90] Based on these effects, the traveling acoustic waves enable rapid fabrication of anisotropic collagen hydrogels containing aligned collagen fibers. On the other hand, we found that standing bulk acoustic waves, which have parallel, periodic acoustic potential peaks and valleys, also influence the collagen self-assembly process and micro- and nanoscale architectures in collagen hydrogels after gelation, while the effects differ from those of traveling acoustic waves. Our study reveals that standing acoustic waves affect the distribution of self-assembled collagen fibers, with higher fiber concentrations in the acoustic potential valleys. Based on this effect, standing acoustic waves have been demonstrated to achieve the quick fabrication of collagen hydrogels containing low and high collagen fiber concentrations in periodic distributions. Additionally, our experimental results show that anisotropic collagen hydrogels containing aligned collagen fibers achieved by acoustic waves can affect the cell arrangement and elongation. Cells cultured in our fabricated hydrogel exhibit elongation along the direction of acoustically aligned collagen fibers.

To investigate the aforementioned acoustic effects and enable rapid in-Petri-dish fabrication of anisotropic collagen hydrogels, we designed customized acoustic devices, which can generate traveling bulk acoustic waves when placing one plate-type piezoelectric transducer in the collagen solution loaded in a Petri dish and generate standing bulk acoustic waves when using a pair of transducers facing each other. Using the design with one transducer, we successfully fabricated anisotropic collagen hydrogels containing directional collagen fibers aligned by traveling wave-induced acoustic streaming. Using the design with a pair of transducers, we demonstrated the ability to increase collagen fiber concentration using the potential valleys of standing acoustic waves and to create periodically and parallelly arranged macroscale bundles densely packed with nanoscale collagen fibers. These experimental results validate the effectiveness of our devices for rapid, in-Petri-dish fabrication of anisotropic collagen hydrogels. Since the resulting collagen distributions depend on the generated acoustic fields, it should be possible to tailor these distributions by controlling the acoustic fields through various approaches, such as changing transducer positions, adjusting excitation signals, and combining traveling and standing waves. We will investigate these strategies in future work to enable the fabrication of hydrogels containing customized collagen distributions.

Compared to other methods for aligning collagen fibers (such as those using external electric fields, microfluidics, and cyclic tensile loading), our acoustic approaches are easy to operate, capable of fabricating anisotropic collagen hydrogels within minutes, and do not require customized chambers for loading collagens. They are compatible with commercial Petri dishes, which are common in research laboratories. With these features, we expect our acoustic approaches to be easily integrated into existing laboratory workflows and combined with other test protocols. Compared to previous bulk acoustic wave-based collagen fiber arrangement methods,[78,79,81] our approach does not require bulky water bath tanks, which are difficult to integrate with inverted microscopes. Moreover, this work more clearly elucidates the mechanisms of collagen self-assembly and fiber alignment induced by traveling and standing acoustic waves, through acoustic field measurements and streaming field visualization. In our future work, we will quantitatively characterize the material properties (such as direction-dependent strength and modulus) of anisotropic collagen hydrogels fabricated using our acoustics-assisted approaches. We will also quantitatively analyze how these anisotropic hydrogels affect cell morphology and migration. Additionally, we will explore the potential applications of our fabrication method for various biomedical research areas, such as tissue model development and hydrogel-based biosensor fabrication. In the long term, we anticipate that our research on acoustics-assisted collagen self-assembly will lead to valuable tools that benefit biomedical researchers working in tissue engineering, cancer cell invasion research, bioprinting, and biomaterials, as well as applications in wound dressings, corneal grafts, and regenerative medicine.

4. Experimental section

4.1 Acoustic test setup and operation

To perform experiments with traveling and standing acoustic waves, we used the setups illustrated in Fig. 2(a). A collagen solution was loaded into a 35 mm-diameter glass-bottom Petri dish (Mattek, USA) to fully cover the glass bottom. For traveling wave generation, our test setup adopted a plate-type piezoelectric transducer (Steiner & Martins, Inc., USA) with dimensions of $26 \times 8 \times 0.7$ mm. The transducer was dipped into the solution loaded in the dish. For standing wave generation, we used a pair of parallelly arranged piezoelectric transducers. To ensure the transducers were perpendicular to the Petri dish's bottom, a customized transducer holder was fabricated *via* three-dimensional printing. Before using the transducers for collagen self-assembly experiments, a network analyzer (E5061B, Keysight) was used to characterize their operating frequencies. Their first- and second-order resonance frequencies were found at 3.09 and 9.60 MHz, respectively. For acoustic wave generation, sinusoidal excitation signals were generated by a function generator (AFG3102, Tektronix), amplified by a power amplifier (A075, E&I), and then sent to the transducers. To perform acoustics-assisted collagen self-assembly and hydrogel fabrication experiments, the acoustic transducers were excited for 5 to 10 min until the completion of collagen gelation. Additionally, the Petri

dish with acoustic transducers could be placed on the microscope stage for real-time monitoring of the acoustic effects on the collagen hydrogel fabrication process. In this study, the thickness of the collagen solution was approximately 1.5 mm. For other thicknesses, our devices can still generate traveling and standing acoustic waves to assist in collagen hydrogel fabrication. However, their performance in arranging collagen fibers will differ, as changes in the solution thickness alter the generated acoustic pressure and streaming fields.

4.2 Laser Doppler vibrometry

To characterize the acoustic field generated in the liquid layer within a Petri dish, we used the test setup illustrated in Fig. 2(b). The piezoelectric transducer was excited by a voltage signal with three-cycle tone bursts modulated by a Hanning window, generated by an arbitrary waveform generator (AFG3102, Tektronix). The excitation signal's center frequency was 3.09 MHz. To measure the generated acoustic fields, a laser Doppler vibrometer (VFX-I-130, Polytec Inc.), equipped with a $10\times$ objective (VIB-A-10$\times$ LENS), was mounted on a three-axis linear motion stage. Its laser beam (with focused laser spot diameter approximately 3 μm) transmitted perpendicularly through the liquid layer in the Petri dish and reflected back from a reflection film placed under the dish. The output voltage signal from the laser Doppler vibrometer was acquired by an oscilloscope (TDS 2014C, Tektronix). This method allowed the acquisition of waveforms containing information about the acoustic waves overlapping with the laser path, similar to approaches used in other studies for characterizing acoustic waves in water.[86] By changing the laser head position using a linear motion stage, the characterization system performed measurements at multiple points in a 6×6 mm area with a step interval of 0.1 mm (*i.e.*, $61\times61 = 3721$ measurement points). At each sensing position, eight waveforms were acquired and averaged to obtain a low-noise waveform. By combining the averaged waveforms for all laser measurement positions, a multi-dimensional time-space wavefield $u(t, x, y)$ was obtained, revealing the propagation of acoustic waves generated in the liquid layer in the Petri dish.

4.3 Particle image velocimetry

To characterize the traveling acoustic wave-induced streaming field, particle image velocimetry experiments were performed. Fluorescent particles with a diameter of 5 μm were used as tracing particles, which were added to the liquid for acoustic streaming characterization. The prepared particle solution was added to the Petri dish, and the acoustic waves were then activated. Due to the drag forces applied to the tracing particles, they were transported following the streaming lines. An inverted microscope equipped with a camera was used to record a video of particle motions. The frames from the acquired video were analyzed using a particle image velocimetry toolbox (PIVlab, version 2.62) in MATLAB R2023b[87,88] to obtain a velocity magnitude field showing the streaming velocity distribution, along with a vector field indicating flow directions at different locations.

4.4 Collagen solution preparation

This study used purified, acid-solubilized rat tail tendon type I collagen (50201, Ibidi GmbH). The collagen stock solution (5 mg mL^{-1}) was diluted to different concentrations, including 0.5, 1, and 2.5 mg mL^{-1}, by adding deionized water, 0.1 N NaOH, and phosphate-buffered saline. For example, to prepare 1 mL of solution with a collagen concentration of 1.0 mg mL^{-1}, 200 μL of collagen stock solution was mixed with 690 μL of deionized water, 20 μL of 0.1 N NaOH for neutralization, and 90 μL of 10$\times$ phosphate-buffered saline. Additionally, the collagen solution preparation was conducted on ice to maintain a low temperature ($\sim 4\,^{\circ}$C).

4.5 Cell culture

The human glioblastoma cell line (U251 cells) was cultured in Dulbecco's Modified Eagle's Medium (DMEM, Genesee Scientific) supplemented with 1% glutamine, 10% fetal bovine serum (FBS) and 1% Penicillin–Streptomycin (30-002-CI, Corning). The cells were maintained at 37 $^{\circ}$C in a humidified incubator with 5% CO$_2$. Passaging was performed twice weekly using 0.05% trypsin-EDTA (sc-363354, Santa Cruz Biotechnology, Inc.), followed by resuspension in the culture medium. Prior to the arrangement of cells within the collagen solution, U251 cells were suspended in the collagen solution at a density of 1×10^6 cells per mL.

4.6 Microscopic imaging

To characterize the collagen fiber morphology, confocal laser scanning microscopy (LSM 880, Zeiss) was performed. Both brightfield and fluorescent images of the fabricated collagen hydrogels were acquired. For fluorescent imaging, the collagen fibers were fluorescently labeled (HY-66019, MedChem Express) after collagen hydrogel fabrication. To analyze collagen fiber orientation in a specific region of the acquired microscopic image, the region of interest was divided into 10×10 subregions. The orientation of the majority of fibers in each subregion was then identified, falling into one of six ranges: 0–30, 30–60, 60–90, 90–120, 120–150, or 150–180 deg.

Author contributions

Yingshan Du: conceived and designed the experiments; the performance experiments with the help of Jiali Li, Teng Li, Luyu Bo, Liang Shen; Chongpeng Qiu: helped with the schematics; Bowen Cai helped with the acoustic field analysis; Yingshan Du: wrote the manuscript with contributions from all authors.

Conflicts of interest

There are no conflicts to declare.

Data availability

The data supporting this study are available upon reasonable request. Please contact the corresponding author for further details.

Additional high-resolution microscopy images and supporting videos related to the collagen experiments. See DOI: **https://doi.org/10.1039/d5ma00271k**.

Acknowledgements

References

1 Y. Li, Y. Liu, R. Li, H. Bai, Z. Zhu, L. Zhu, C. Zhu, Z. Che, H. Liu, J. Wang and L. Huang, *Mater. Des.*, 2021, **210**, 110049.

2 Y. Wang, Z. Wang and Y. Dong, *ACS Biomater. Sci. Eng.*, 2023, **9**, 1132–1150.

3 K. Lin, D. Zhang, M. H. Macedo, W. Cui, B. Sarmento and G. Shen, *Adv. Funct. Mater.*, 2019, **29**, 1804943.

4 D. Kim, S. Eom, S. M. Park, H. Hong and D. S. Kim, *Sci. Rep.*, 2019, **9**, 14915.

5 J. N. Ouellette, C. R. Drifka, K. B. Pointer, Y. Liu, T. J. Lieberthal, W. J. Kao, J. S. Kuo, A. G. Loeffler and K. W. Eliceiri, *Bioengineering*, 2021, **8**, 17.

6 A. Dewle, N. Pathak, P. Rakshasmare and A. Srivastava, *ACS Biomater. Sci. Eng.*, 2020, **6**, 779–797.

7 J. Mao, L. Chen, Z. Cai, S. Qian, Z. Liu, B. Zhao, Y. Zhang, X. Sun and W. Cui, *Adv. Funct. Mater.*, 2022, **32**, 2111003.

8 J. Sapudom, S. Karaman, B. C. Quartey, W. K. E. Mohamed, N. Mahtani, A. Garcia-Sabaté and J. Teo, *Adv. Sci.*, 2023, **10**, 2301353.

9 J. M. Szulczewski, D. R. Inman, M. Proestaki, J. Notbohm, B. M. Burkel and S. M. Ponik, *Acta Biomater.*, 2021, **129**, 96–109.

10 S. Brassart-Pasco, S. Brézillon, B. Brassart, L. Ramont, J.-B. Oudart and J. C. Monboisse, *Front. Oncol.*, 2020, **10**, 397.

11 Y. Yang, Y. Fan, H. Zhang, Q. Zhang, Y. Zhao, Z. Xiao, W. Liu, B. Chen, L. Gao, Z. Sun, X. Xue, M. Shu and J. Dai, *Biomaterials*, 2021, **269**, 120479.

12 A. Schwab, C. Hélary, R. G. Richards, M. Alini, D. Eglin and M. D'Este, *Mater. Today Bio*, 2020, **7**, 100058.

13 Q. Zhang, P. Nguyen, J. C. Burrell, J. Zeng, S. Shi, R. M. Shanti, G. Kulischak, D. K. Cullen and A. D. Le, *npj Regener. Med.*, 2021, **6**, 1–14.

14 J. Shen, Z. Wang, W. Zhao, Y. Fu, B. Li, J. Cheng, Y. Deng, S. Li and H. Li, *Reprod. Biol.*, 2022, **22**, 100705.

15 X. Chen, D. Chen, E. Ban, K. C. Toussaint, P. A. Janmey, R. G. Wells and V. B. Shenoy, *Proc. Natl. Acad. Sci. U. S. A.*, 2022, **119**, e2116718119.

16 Z. Amidzadeh, S. Yasami-Khiabani, H. Rahimi, S. Bonakdar, D. Shams, M. Habibi-Anbouhi, M. Golkar and M. A. Shokrgozar, *J. Cell. Mol. Med.*, 2022, **26**, 5929–5942.

17 N. Mahmoodi, J. Ai, Z. Hassannejad, S. Ebrahimi-Barough, E. Hasanzadeh, H. Nekounam, A. R. Vaccaro and V. Rahimi-Movaghar, *Sci. Rep.*, 2021, **11**, 21722.

18 P. Sawadkar, P. Sibbons, T. Ahmed, L. Bozec and V. Mudera, *ACS Biomater. Sci. Eng.*, 2019, **5**, 5218–5228.

19 K. S. Koeck, S. Salehi, M. Humenik and T. Scheibel, *Adv. Funct. Mater.*, 2022, **32**, 2112238.

20 M. Fuest, G. H.-F. Yam, J. S. Mehta and D. F. Duarte Campos, *Bioengineering*, 2020, **7**, 71.

21 D. B. Burr, in *Basic and Applied Bone Biology*, ed. D. B. Burr and M. R. Allen, Academic Press, San Diego, 2nd edn, 2019, pp. 3–26.

22 X. Cui, K. Breitenkamp, M. G. Finn, M. Lotz and D. D. D'Lima, *Tissue Eng., Part A*, 2012, **18**, 1304–1312.

23 K. Henriksen and M. A. Karsdal, in *Biochemistry of Collagens, Laminins and Elastin*, ed. M. A. Karsdal, Academic Press, San Diego, 3rd edn, 2024, pp. 1–11.

24 G. Y. Liu, R. Agarwal, K. R. Ko, M. Ruthven, H. T. Sarhan and J. P. Frampton, *Sci. Rep.*, 2017, **7**, 9628.

25 L. Robert, J. M. Legeais, A. M. Robert and G. Renard, *Pathol. Biol.*, 2001, **49**, 353–363.

26 J. Hu, Y. Song, C. Zhang, W. Huang, A. Chen, H. He, S. Zhang, Y. Chen, C. Tu, J. Liu, X. Xuan, Y. Chang, J. Zheng and J. Wu, *ACS Appl. Bio Mater.*, 2020, **3**, 965–976.

27 M. G. McCoy, J. M. Wei, S. Choi, J. P. Goerger, W. Zipfel and C. Fischbach, *ACS Biomater. Sci. Eng.*, 2018, **4**, 2967–2976.

28 P. V. Taufalele, J. A. VanderBurgh, A. Muñoz, M. R. Zanotelli and C. A. Reinhart-King, *PLoS One*, 2019, **14**, e0216537.

29 J. D. Currey, *Bones: Structure and Mechanics*, Princeton University Press, Princeton, 2002.

30 J. M. Lee, S. K. Q. Suen, W. L. Ng, W. C. Ma and W. Y. Yeong, *Macromol. Biosci.*, 2021, **21**, 2000280.

31 X. Luo, S. Zhang, B. Luo and H. Li, *Int. J. Biol. Macromol.*, 2021, **185**, 77–86.

32 S. Yunoki, H. Hatayama, M. Ebisawa, E. Kondo and K. Yasuda, *J. Biomed. Mater. Res., Part B*, 2019, **107**, 1011–1023.

33 A. Ahmed, I. M. Joshi, M. Mansouri, N. N. N. Ahamed, M.-C. Hsu, T. R. Gaborski and V. V. Abhyankar, *Am. J. Physiol. Cell Physiol.*, 2021, **320**, C1112–C1124.

34 A. Ahmed, I. M. Joshi, S. Larson, M. Mansouri, S. Gholizadeh, Z. Allahyari, F. Forouzandeh, D. A. Borkholder, T. R. Gaborski and V. V. Abhyankar, *Adv. Mater. Technol.*, 2021, **6**, 2001186.

35 F. Giacomini, D. Baião Barata, H. Suk Rho, Z. Tahmasebi Birgani, C. van Blitterswijk, S. Giselbrecht, R. Truckenmüller and P. Habibović, *Adv. Healthcare Mater.*, 2024, **13**, 2303672.

36 G. Spiaggia, P. Taladriz-Blanco, D. Septiadi, R. D. Ortuso, A. Lee, V. Trappe, B. Rothen-Rutishauser and A. Petri-Fink, *ACS Appl. Bio Mater.*, 2021, **4**, 8316–8324.

37 B. Lanfer, U. Freudenberg, R. Zimmermann, D. Stamov, V. Körber and C. Werner, *Biomaterials*, 2008, **29**, 3888–3895.

38 I. M. Joshi, M. Mansouri, A. Ahmed, R. A. Simon, P. E. Bambizi, D. E. Desa, T. M. Elias, E. B. Brown and V. V. Abhyankar, *bioRxiv*, 2023, preprint, DOI: **10.1101/2023.07.09.548253**.

39 P. Lee, R. Lin, J. Moon and L. P. Lee, *Biomed. Microdevices*, 2006, **8**, 35–41.

40 C.-Y. Su, A. Burchett, M. Dunworth, J. S. Choi, A. J. Ewald, E. H. Ahn and D.-H. Kim, *Biomaterials*, 2021, **275**, 120922.

41 L. M. Dedroog, O. Deschaume, C. J. G. Abrego, E. Koos, Y. de Coene, A. Vananroye, W. Thielemans, C. Bartic and M. P. Lettinga, *Acta Biomater.*, 2022, **150**, 128–137.

42 B. A. Nerger, P.-T. Brun and C. M. Nelson, *Soft Matter*, 2019, **15**, 5728–5738.

43 D. V. Shepherd, J. H. Shepherd, S. Ghose, S. J. Kew, R. E. Cameron and S. M. Best, *APL Mater.*, 2015, **3**, 014902.

44 A. Dewle, P. Rakshasmare and A. Srivastava, *ACS Appl. Bio Mater.*, 2021, **4**, 1238–1251.

45 Z. Chen, X. Liu, J. You, Y. Song, E. Tomaskovic-Crook, G. Sutton, J. M. Crook and G. G. Wallace, *Acta Biomater.*, 2020, **113**, 360–371.

46 M. Lei, X. Qu, H. Wan, D. Jin, S. Wang, Z. Zhao, M. Yin, G. F. Payne and C. Liu, *Sci. Adv.*, 2022, **8**, eabl7506.

47 Z. Chen, X. Liu, J. You, E. Tomaskovic-Crook, Z. Yue, A. Talaei, G. Sutton, J. Crook and G. Wallace, *J. Biomed. Mater. Res., Part A*, 2023, **111**, 1151–1160.

48 M. Antman-Passig, S. Levy, C. Gartenberg, H. Schori and O. Shefi, *Tissue Eng., Part A*, 2017, **23**, 403–414.

49 D. Vader, A. Kabla, D. Weitz and L. Mahadevan, *PLoS One*, 2009, **4**, e5902.

50 J. Gessmann, D. Seybold, E. Peter, T. A. Schildhauer and M. Köller, *Tissue Eng., Part C*, 2016, **22**, 30–37.

51 W. Shi, J. Huang, R. Fang and M. Liu, *ACS Appl. Mater. Interfaces*, 2020, **12**, 5177–5194.

52 B. Xu, M.-J. Chow and Y. Zhang, *Int. J. Biomater.*, 2011, **2011**, e172389.

53 M. Santhosh, J.-H. Choi and J.-W. Choi, *Nanomaterials*, 2019, **9**, 1293.

54 M. Antman-Passig and O. Shefi, *Nano Lett.*, 2016, **16**, 2567–2573.

55 L. Hao and H. Mao, *Biomater. Sci.*, 2023, **11**, 6384–6402.

56 K. A. Tran, Y. Jin, J. Bouyer, B. J. DeOre, Ł. Suprewicz, A. Figel, H. Walens, I. Fischer and P. A. Galie, *Biomater. Sci.*, 2022, **10**, 2237–2247.

57 I. M. Basurto, M. T. Mora, G. M. Gardner, G. J. Christ and S. R. Caliari, *Biomater. Sci.*, 2021, **9**, 4040–4053.

58 D. Pei, M. Wang, W. Li, M. Li, Q. Liu, R. Ding, J. Zhao, A. Li, J. Li, F. Xu and G. Jin, *Acta Biomater.*, 2020, **112**, 202–212.

59 A. Ahmed, I. M. Joshi, M. R. Goulet, J. A. Vidas, A. M. Byerley, M. Mansouri, S. W. Day and V. V. Abhyankar, *J. Visualized Exp.*, 2022, **187**, DOI: 10.3791/64457.

60 A. Marzo, S. A. Seah, B. W. Drinkwater, D. R. Sahoo, B. Long and S. Subramanian, *Nat. Commun.*, 2015, **6**, 8661.

61 J.-C. Hsu and Y.-D. Lin, *Sens. Actuators, A*, 2019, **300**, 111651.

62 K. Kolesnik, M. Xu, P. V. S. Lee, V. Rajagopal and D. J. Collins, *Lab Chip*, 2021, **21**, 2837–2856.

63 Q. Wang, Z. Ding, G. Wong, J. Zhou and A. Riaud, *Anal. Chem.*, 2023, **95**, 6253–6260.

64 J. Li, A. Crivoi, X. Peng, L. Shen, Y. Pu, Z. Fan and S. A. Cummer, *Commun. Phys.*, 2021, **4**, 1–8.

65 A. G. Guex, N. Di Marzio, D. Eglin, M. Alini and T. Serra, *Mater. Today Bio*, 2021, **10**, 100110.

66 M. Wu, Y. Ouyang, Z. Wang, R. Zhang, P.-H. Huang, C. Chen, H. Li, P. Li, D. Quinn, M. Dao, S. Suresh, Y. Sadovsky and T. J. Huang, *Proc. Natl. Acad. Sci. U. S. A.*, 2017, **114**, 10584–10589.

67 F. Guo, Z. Mao, Y. Chen, Z. Xie, J. P. Lata, P. Li, L. Ren, J. Liu, J. Yang, M. Dao, S. Suresh and T. J. Huang, *Proc. Natl. Acad. Sci. U. S. A.*, 2016, **113**, 1522–1527.

68 D. Ahmed, A. Ozcelik, N. Bojanala, N. Nama, A. Upadhyay, Y. Chen, W. Hanna-Rose and T. J. Huang, *Nat. Commun.*, 2016, **7**, 11085.

69 M. S. Gerlt, P. Ruppen, M. Leuthner, S. Panke and J. Dual, *Lab Chip*, 2021, **21**, 4487–4497.

70 V. M. Jooss, J. S. Bolten, J. Huwyler and D. Ahmed, *Sci. Adv.*, 2022, **8**, eabm2785.

71 P. Zhang, C. Chen, F. Guo, J. Philippe, Y. Gu, Z. Tian, H. Bachman, L. Ren, S. Yang, Z. Zhong, P.-H. Huang, N. Katsanis, K. Chakrabarty and T. Jun Huang, *Lab Chip*, 2019, **19**, 3397–3404.

72 A. Ahsan Nawaz, D. Soteriou, C. K. Xu, R. Goswami, M. Herbig, J. Guck and S. Girardo, *Lab Chip*, 2023, **23**, 372–387.

73 T. Franke, S. Braunmüller, L. Schmid, A. Wixforth and D. A. Weitz, *Lab Chip*, 2010, **10**, 789–794.

74 S. Bhattacharya, T. Banerjee, Y. Miao, H. Zhan, P. N. Devreotes and P. A. Iglesias, *Sci. Adv.*, 2020, **6**, eaay7682.

75 S. van den Driesche, V. Rao, D. Puchberger-Enengl, W. Witarski and M. J. Vellekoop, *Sens. Actuators, B*, 2012, **170**, 207–214.

76 Y. C. Kim, P. R. S. Vijayaratnam, P. Blanloeuil, R. A. Taylor and T. J. Barber, *Ultrasound Med. Biol.*, 2023, **49**, 961–969.

77 J. G. Lee, R. R. Raj, C. P. Thome, N. B. Day, P. Martinez, N. Bottenus, A. Gupta and C. Wyatt Shields IV, *Small*, 2023, **19**, 2300409.

78 E. G. Norris, D. Dalecki and D. C. Hocking, *Appl. Sci.*, 2020, **10**, 2907.

79 E. G. Norris, D. Dalecki and D. C. Hocking, *Mater. Today Bio*, 2019, **3**, 100018.

80 P. Zhang, J. Rufo, C. Chen, J. Xia, Z. Tian, L. Zhang, N. Hao, Z. Zhong, Y. Gu, K. Chakrabarty and T. J. Huang, *Nat. Commun.*, 2021, **12**, 3844.

81 E. G. Norris, J. Majeski, S. E. Wayson, H. Coleman, R. Choe, D. Dalecki and D. C. Hocking, *Mater. Res. Express*, 2019, **6**, 125410.

82 W.-H. Huang, S.-L. Ding, X.-Y. Zhao, K. Li, H.-T. Guo, M.-Z. Zhang and Q. Gu, *Mater. Today Bio*, 2023, **20**, 100639.

83 C. Chen, Y. Gu, J. Philippe, P. Zhang, H. Bachman, J. Zhang, J. Mai, J. Rufo, J. F. Rawls, E. E. Davis, N. Katsanis and T. J. Huang, *Nat. Commun.*, 2021, **12**, 1118.

84 J. Tien and Y. W. Dance, *Adv. Healthcare Mater.*, 2021, **10**, 2001028.

85 X. Cheng, U. A. Gurkan, C. J. Dehen, M. P. Tate, H. W. Hillhouse, G. J. Simpson and O. Akkus, *Biomaterials*, 2008, **29**, 3278–3288.

86 R. Longo, S. Vanlanduit, G. Arroud and P. Guillaume, *Sensor*, 2015, **15**, 19925–19936.

87 W. Thielicke and R. Sonntag, *J. Open Res. Softw.*, 2021, **9**, 12.

88 W. Thielicke and E. J. Stamhuis, *J. Open Res. Softw.*, 2014, **2**, e30.

89 C. Mu, D. Li, W. Lin, Y. Ding and G. Zhang, *Biopolymers*, 2007, **86**, 282–287.

90 D. Fan, J. Xing, W. Xue, C. Zhu, X. Ma and R. Ma, *Chin. J. Chem.*, 2011, **29**, 1811–1816.

91 Z. Tian, S. Yang, P.-H. Huang, Z. Wang, P. Zhang, Y. Gu, H. Bachman, C. Chen, M. Wu, Y. Xie and T. J. Huang, *Sci. Adv.*, 2019, **5**, eaau6062.